

Significant Photoluminescence Improvements from Bulk Germanium-Based Thin Films with Ultra-low Threading Dislocation Densities

Liming Wang¹, Gideon Kassa², Jifeng Liu², and Guangrui Xia^{1*}

¹ Department of Materials Engineering, The University of British Columbia, Vancouver, BC V6T 1Z4,
Canada

² Thayer School of Engineering, Dartmouth College, Hanover, New Hampshire 03766, United States

*Corresponding author: guangrui.xia@ubc.ca

Abstract

Bulk Ge crystals, characterized by significantly lower threading dislocation densities (TDD) than their epitaxial counterparts, emerge as optimal candidates for studying and improving Ge laser performance. Our study focused on the Ge thickness and TDD impacts on Ge's photoluminescence (PL). The PL peak intensity of a bulk Ge sample (TDD = 6000 cm⁻², n-doping = 10¹⁶ cm⁻³) experiences a remarkable 32-fold increase as the thickness is reduced from 535 μm to 2 μm. This surpasses the PL peak intensity of a 0.75 μm thick epi-Ge on Si (biaxial tensile strain= 0.2 %, n-doping = 10¹⁹ cm⁻³) by a factor of 2.5. Furthermore, the PL peak intensity of a 405 μm thick zero-TDD bulk Ge sample (n-doping = 5 × 10¹⁷ cm⁻³) is ten times that of the 0.75 μm thick epi-Ge, rising to twelve times when thinned to 1 μm. The TDD reduction method is highly effective, which relaxes the requirements of high n-doping and stress in enhancing Ge laser performance and thus reduces the side effects of high optical absorption, high non-radiative recombination, bandgap narrowing, and large footprints associated with these two techniques.

1. Introduction

Silicon (Si)-compatible on-chip lasers are important across diverse applications such as optical computing¹, bio-chemical sensing², quantum computing³, and on-chip and off-chip optical communication⁴.⁵ Over the past few decades, researchers worldwide have dedicated extensive efforts to identifying viable solutions for a Si-compatible light-emitting material system.⁶⁻⁸ A promising avenue in addressing this challenge is the adoption of germanium (Ge), recognized for its exceptional compatibility with Si, making it a well-suited semiconductor for monolithic integration. Furthermore, Ge has already found applications in MOSFETs⁹⁻¹⁰ and Si photonics, serving as detectors¹¹⁻¹² and modulators¹³⁻¹⁴. However, Ge is similar to Si, being an indirect bandgap material. Notably, the indirect bandgap of Ge measures 0.664 eV at the L valleys, while the direct bandgap is 0.800 eV at the Γ valley, exhibiting a difference of only 136 meV at room temperature.¹⁵ Ge can be transformed into a direct or pseudo-direct bandgap material through bandgap engineering via tensile strains and n-doping, providing a key advancement facilitating efficient light emission.¹⁶ Introducing tensile strain to Ge is pivotal in swiftly reducing the minima of the Γ valley compared to the L valley, effectively narrowing the bandgap. To address the residual difference between the direct and indirect gaps in tensile-strained Ge, electrons are introduced into the L valleys via n-type doping. A milestone in developing Ge on-chip lasers was achieved in 2012 by demonstrating the first electrically pumped Ge laser.¹⁷ The early Ge lasers featured an n-type doping concentration of $4 \times 10^{19} \text{ cm}^{-3}$ and a tensile strain of 0.2%. However, initial Ge lasers faced challenges, including a high threshold current of approximately 280 kA/cm² and an efficiency ranging from 0.5% to 4%, thus presenting obstacles for practical applications.

Theoretical studies focusing on Ge-on-Si lasers suggested that remarkable improvements can be achieved through laser structure design optimization, stress engineering, and TDD reduction.¹⁸⁻¹⁹ The optimized configuration is projected to attain a threshold current density of 3.7 kA/cm², a threshold current of 5 mA, and a differential quantum efficiency of 64.8%.¹⁸ Common commercial compound semiconductor lasers typically exhibit wall-plug efficiencies of 20-50%. The potential

efficiency of the optimized Ge laser, reaching 43.8%, presents a compelling case for further exploration and research in the realm of Ge lasers.

Despite their potential, Ge lasers encounter a significant hurdle in epitaxial Ge (epi-Ge)-based lasers due to the high TDD in the range of 10^6 to 10^{10} cm^{-2} .²⁰ This elevated TDD directly impacts the performance metrics of Ge lasers, resulting in higher threshold currents and reduced efficiencies attributed to non-radiative recombination processes.²¹ In contrast, bulk Ge crystals have ultra-low TDD of $\leq 10^4$ cm^{-2} . The best commercial Ge wafers have zero TDD measured by etch pit density (EPD). This substantial TDD reduction positions bulk Ge as an intriguing material for exploring the ultimate potentials of Ge on-chip lasers and different Ge laser improvement strategies.

Up to date, epi-Ge has been the choice of all previous Ge laser studies due to the ease of obtaining micron or sub-micron scale thickness needed for on-chip applications. Most ultra-high-quality bulk Ge crystals are Ge wafers, whose thicknesses are generally several hundred micrometers. These thicknesses are not desired for on-chip applications due to the large dimension and the increased absorption resulting from its indirect bandgap.²²⁻²³ Overcoming the obstacles requires innovative approaches to achieve thickness reduction to a micron-scale without compromising the material's structural integrity, surface roughness, and defect density. A smart-cut method²⁴ has been proposed for acquiring a Ge thin film on a Si substrate. However, heavy ion implantation introduces defects in Ge²⁵⁻²⁶. Solution-based methods, such as wet etching for thinning Ge, offer a more cost-effective and accessible alternative without any ion implantation damage. Additionally, Ge thin films obtained through wet etching are fully relaxed, allowing us to eliminate the influence of tensile strain, which is inevitable during the wafer bonding process in the smart-cut method²⁷. One study in 2010 achieved Ge thin films from Ge wafers with a minimum thickness of 28 μm by wet etching.²⁸ The bulk-Ge-based thin film thickness record was recently updated by our work to be 4.1 μm using an $\text{HCl-H}_2\text{O}_2\text{-H}_2\text{O}$ solution.²⁹ Due to the difficulty in obtaining micron-scale Ge thin films from bulk Ge, Ge thin films with ultra-low TDD have not been well studied for light emission purposes, which was addressed in this work.

In our study, we successfully fabricated micron-scale Ge thin films with good integrity. The PL of both an epi-Ge control sample and thinned bulk Ge samples were measured to elucidate the impacts of the thickness, TDD, doping concentration, surface roughness, and heating effect.

2. Experiment

2.1 Samples selection

A specific bench-marking epi-Ge on Si sample was chosen as the control sample for this study. Detailed information about this sample has been previously documented in Ref. 28, where it was named P-NA-off. This bench-marking epi-Ge has 5% higher PL intensity than that of the MIT Ge sample. Notably, the MIT Ge sample, which was a delta-doped blanket n⁺ Ge film, achieved the best performance to date for a room temperature operated electrically pumped Ge laser when the same growth method was applied to selective growth followed by chemical mechanical polishing.³⁰ Ge wafers from two sources were selected as the starting materials. The first was a 4-inch n-type Ge wafer purchased from University Wafer, Inc. (UW) with a typical TDD of 6000 cm⁻², as previously measured and reported in the literature.²⁹ The second wafer was a 4-inch n-type (with a resistivity of ≤ 0.01 Ohms*cm at 295 K), single-side polished (100) Ge wafer sourced from Umicore. Notably, this wafer boasts zero TDD measured by etch-pit density (EPD).

Table 1. The information on bulk Ge from UW and Umicore and epi-Ge on Si

	Thickness (μm)	Tensile strain	P concentration (cm^{-3})	Sq (nm)	TDD (cm^{-2})
UW wafer	535	0	1e16	1.6	~ 6000
Umicore wafer	405	0	5e17	1.0 (polished side)	0
				8.2 (unpolished side)	
Epi-Ge on Si	0.75	0.2 % (biaxial)	1e19	0.8	~ 1e8

2.2 Bulk Ge thinning with wet etching

The UW wafers and Umicore wafers were cut into small pieces before the wet etching. HCl-H₂O₂-H₂O solutions with a volume ratio of 1:1:5 were chosen for the wet etching according to our

previous wet etching study that produced 535- μm -thick Ge thin films down to 4.1 μm with good integrity and no increase in the TDD²⁹.

2.3 Thin Film Characterizations

The thickness of the Ge thin film was measured using a Nikon ECLIPSE LV150 optical microscope equipped with length measurement capabilities. Simultaneously, 3D optical profiler images and rough mean square surface roughness (Sq) of the Ge samples were measured using an optical interferometer (Filmetrics Profilm3D optical surface profiler). To explore the PL properties of Ge, a Horiba LabRAM HR Evolution instrument was employed, featuring an InGaAs photodetector cooled with liquid nitrogen. In this setup, a 1064 nm laser was applied to all samples, a 300 gr/mm grating was used, and a 50X objective lens was utilized. The acquisition time for each spot was set at 3 seconds. Different filters were used to attenuate the excitation laser power before it entered the sample, which translated to 5, 10, and 25% of the original laser power of about 20 mW on the sample surface without any filtering. The choice of laser power was to achieve a balance between a good signal-noise ratio and mitigating the heating effect. The localized heating on the sample may indeed facilitate increased electron injection into the conduction band, resulting in higher PL intensity and a redshift in the PL peak. However, it's crucial to minimize the heating effect to accurately assess the true PL of the sample, without interference from heating-induced changes. A 10% laser power was employed for most measurements with a satisfactory balance between the signal strength and minimal heating. By comparing the PL peak positions, we observed that the PL peaks with 5% and 10% laser power were similar at 1536 nm, but both were smaller than those with 25% laser power by 22 nm as seen in Fig. 7 (c). This indicated that the heating effect from 10% laser power was negligible. In the figures below, the default measurement laser power condition was 10% laser power unless otherwise noted. In cases where UW bulk Ge failed to yield sufficient signal at 10%, a 25% laser power was utilized. Additionally, a 5% laser power reduced the heating effect, particularly in very thin regions near the edges, where heating effects can be more pronounced.

3. Results and discussion

3.1 The UW Ge before and after etching

The initial thickness of the UW Ge wafer, depicted in Figure 1a, measured 535 μm . Following a 52-hour wet etching process with HCl-H₂O₂-H₂O (1:1:5), the thickness of the Ge was successfully reduced to 2 μm , as illustrated in Figure 1b. The photograph of the as-prepared UW Ge thin film, shown in Figure 1c, reveals a mirror-like surface where the reflection of the tweezers is visible. 3D optical profilometer images, acquired through an optical interferometer after the wet etching, are presented in Figure 1d. These images indicate a S_q of 8.2 ± 2.8 nm.

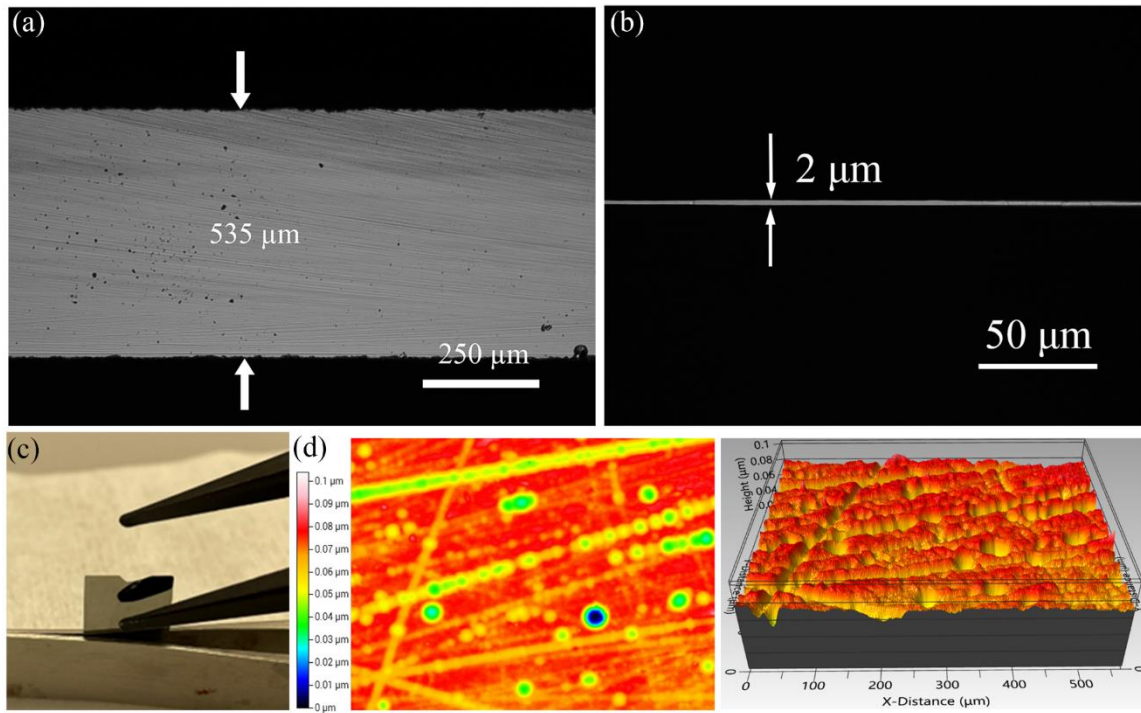


Figure 1. (a) The thickness of the UW bulk Ge wafer before etching, (b) the thickness of the as-prepared UW Ge thin film after wet etching, (c) the photo of as-prepared UW Ge thin film, (d) the 3D optical profilometer image of the UW Ge thin film, $S_q = 8.2 \pm 2.8$ nm.

3.2 PL of the UW Ge with different thicknesses

However, the thickness of the UW Ge thin film edges exhibits non-uniformity, resulting in a thickness gradient from top to bottom, as depicted in Figure 2a. The photo of the side view of the UW Ge thin film is presented in Figure 2b. Figures 2c and 2d show the thin film's thickness

variation from 2 μm near the top edge to 58 μm near the bottom part. The thickness increases with a rate of 4.5 μm per 100 μm position change from the top edge. This unique thickness profile provides an excellent opportunity for studying the impact of Ge thickness.

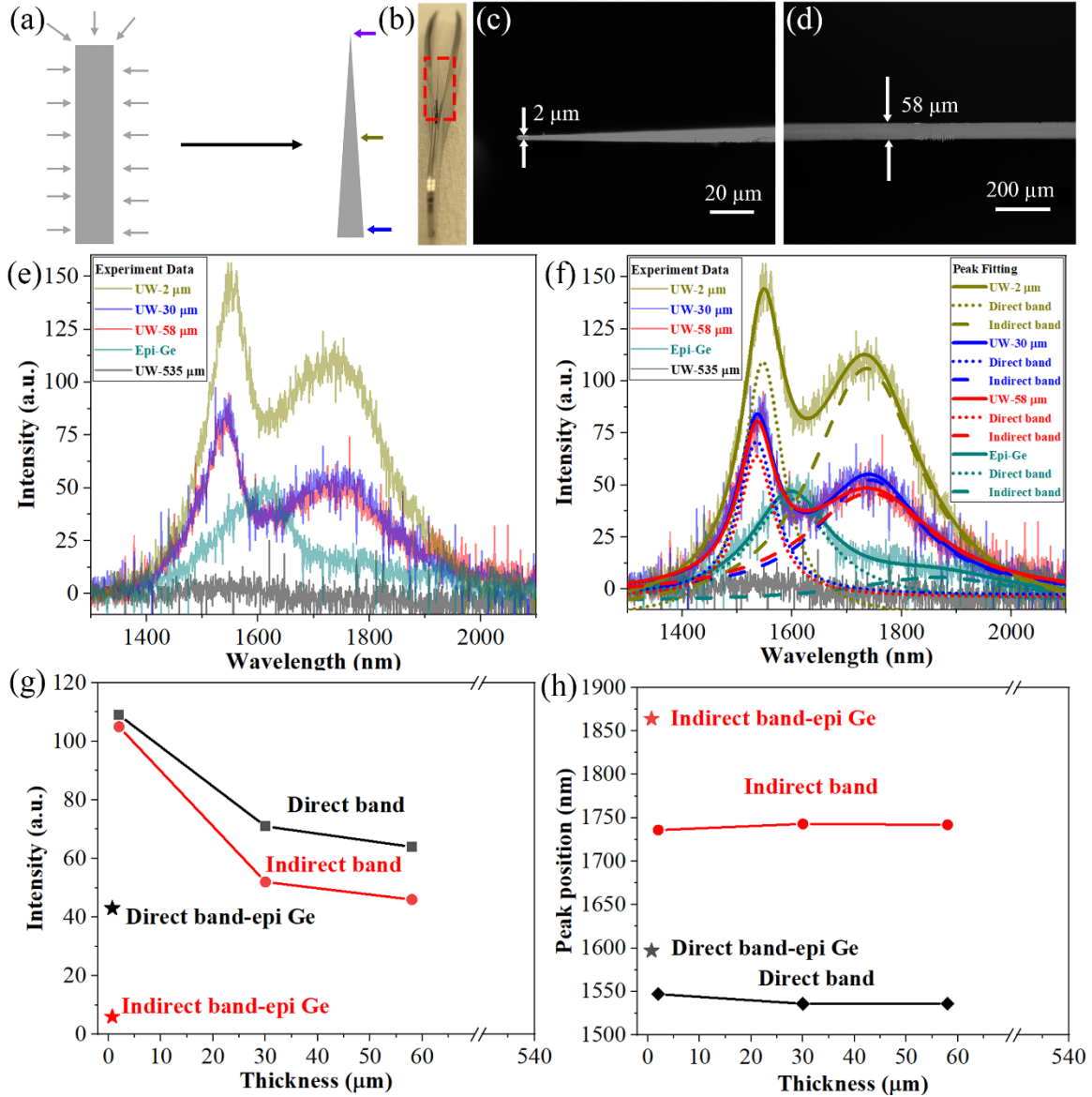


Figure 2. PL measurements were conducted with 10 % of the laser power. (a) The mechanism of the Ge thin film thickness variation, (b) the side view photo of the Ge thin film held by a tweezer, (c) the top part of the Ge thin film from the top, (d) the bottom part of the Ge thin film, (e) the measured PL from the epi-Ge and UW Ge with different thicknesses, (f) the fitted PL peaks from the epi-Ge and UW Ge with different

thicknesses(except for UW Ge-535 μm), (fitted PL peaks are shown except for UW Ge-535 μm), (g) the PL intensity vs. UW Ge thickness, and (h) the PL peak position vs. UW Ge thickness.

After the wet etching, PL measurements were conducted with 10 % of the laser power at different locations on the thin film with thicknesses of 2, 30, and 58 μm , respectively, as illustrated in Figure 2a. Figure 2e compares the UW Ge samples and the epi-Ge on Si. The epi-Ge used in this experiment, comparable to the PL achieved in the previously reported MIT sample³⁰, exhibits two distinct PL peaks after peak finding and fitting. One represents the direct band emission at approximately 1597 nm, and the other corresponds to the indirect band emission at around 1864 nm. The red-shifted direct band emission at 1597 nm, in contrast to the expected 1550 nm from relaxed Ge, is attributed to a biaxial tensile strain of 0.2% and heavy n-doping of $1\text{e}19\text{ cm}^{-3}$ in the epi-Ge³⁰.

In contrast, the UW bulk Ge (535 μm) shows no observable peaks in the PL measurements (Figure 2e). However, remarkably, the PL becomes observable after thinning the film to 58 μm , and its intensity surpasses that of epi-Ge (Figure 2e). The associated direct peak position is approximately 1536 nm, closely aligning with literature reports at 1540 nm³¹. This alignment suggests that using 10 % of the laser power is suitable for minimizing heating effects during PL measurements. The PL intensity increases more when the thickness is reduced to 30 μm . When the thickness decreases from 58 to 2 μm , the intensity from the direct band is 1.7 times that of the UW-58 μm , which is 2.5 times higher than epi-Ge.

Notably, the thickness of UW Ge emerges as a crucial factor influencing the PL spectra. In instances of substantial thickness, the PL of UW-535 μm is obscured due to self-absorption from the indirect band²⁹. However, reducing the thickness to less than 60 μm diminishes self-absorption, significantly increasing the PL signal. A comparison between UW-58 μm and epi-Ge reveals that, despite epi-Ge having 1000 times higher P doping concentration and 0.2% tensile strain, the PL from UW-58 μm surpasses that of epi-Ge. This unexpected outcome underscores the prominence of TDD over n-type doping concentration in improving PL intensities.

3.3 PL of the UW Ge with a higher excitation laser power

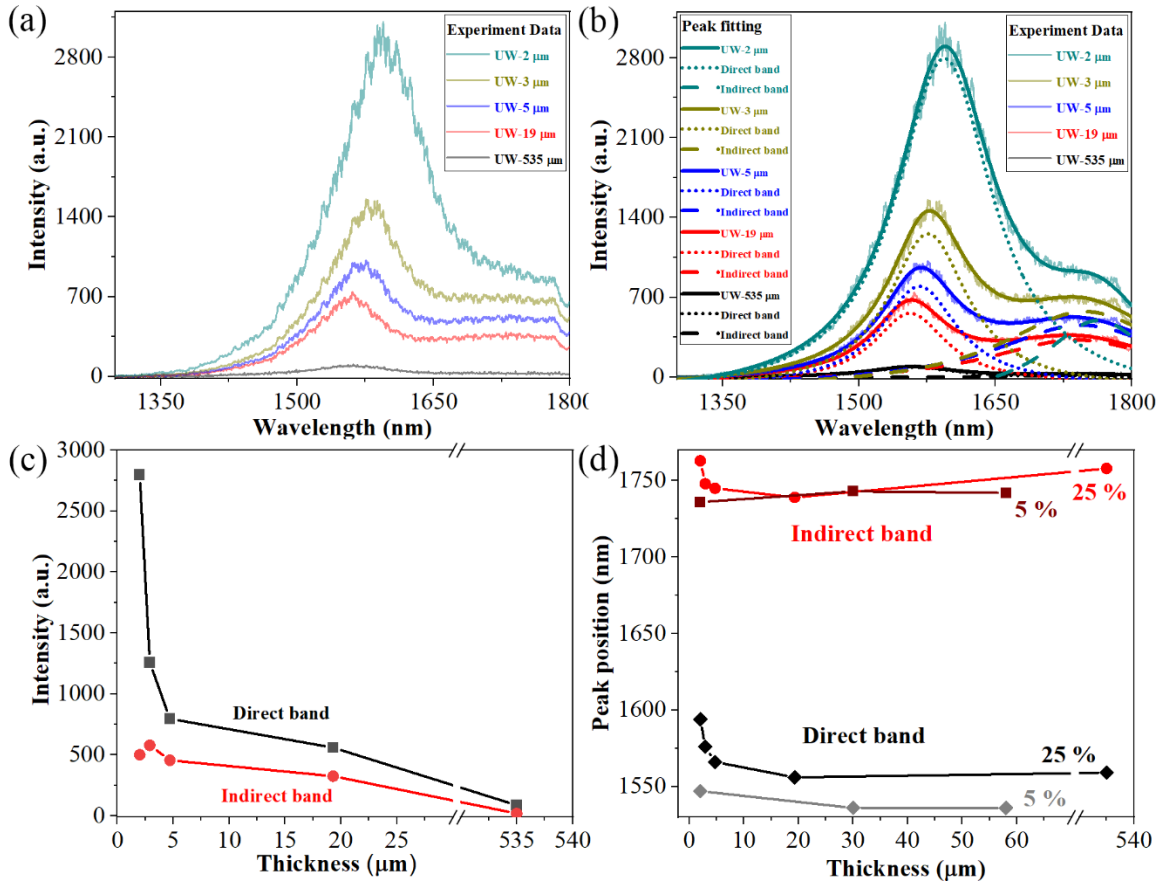


Figure 3. (a) The PL spectra of UW Ge with different thicknesses with a 25 % laser power, (b) the fitted PL peaks of UW Ge with different thicknesses with a 25 % laser power, (c) the PL intensity vs. Ge thickness with a 25 % laser power, and (d) the PL peak position vs. Ge thickness with a 5 % laser power and a 25 % laser power.

A comprehensive linear scan was conducted from the top down using a PL system to investigate further the impact of thickness, particularly in the 2-20 μm range. As depicted in Figure 2c, the thickness increases by 4.5 μm for every 100 μm distance, effectively translating the distance from the PL measurement into a measure of thickness. For a comprehensive comparison with UW-535 μm, the power entering the sample was increased to 25% of the laser power to ensure an adequate PL signal for UW-535 μm. Notably, as the thickness decreases, the PL intensity consistently increases. Compared to UW-535 μm, the UW-2 μm exhibits a remarkable 32-fold increase in the

PL intensity, emphasizing a significant enhancement in PL. It's crucial to note that the heating effect plays a pivotal role in the thinner regions. With a higher temperature, more electrons gain enough energy to occupy the direct valley, which is evident in the dramatic increase in direct emission, a decrease in indirect emission, and a peak shift from 1556 nm to 1594 nm, observed as the thickness reduces from 20 μm to 2 μm .

3.4 PL of the Umicore Ge with different thicknesses

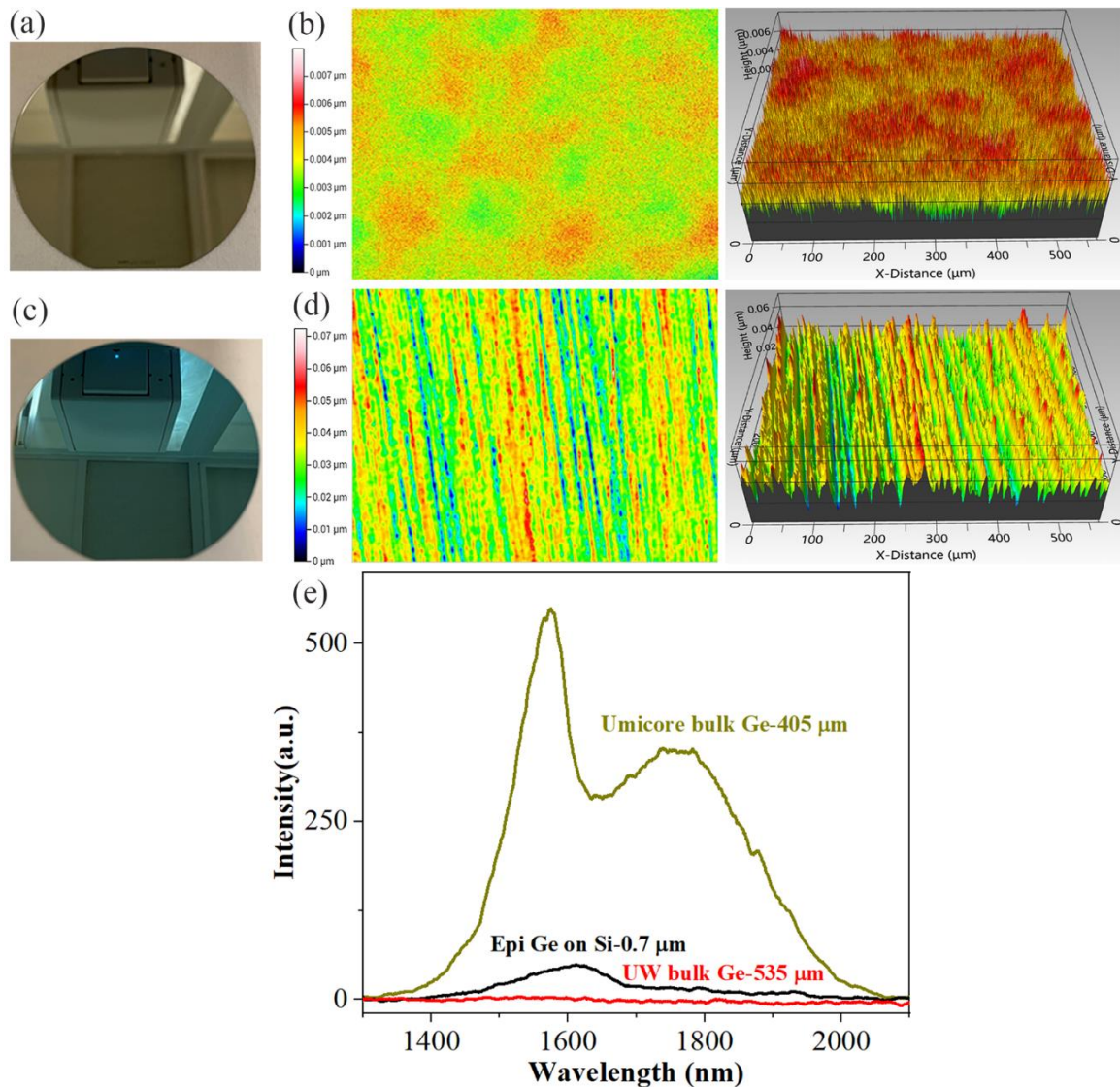


Figure 4. (a) The photo of the Umicore bulk Ge wafer, (b) the 3D optical profilometer image of the Umicore bulk Ge from the polished side, (c) the photo of the unpolished side of Umicore bulk Ge wafer with a SiN

coating, (d) the 3D optical profilometer image of the Umicore bulk Ge from the unpolished side, and (e) a comparison of PL among UW bulk Ge, epi-Ge on Si, and Umicore bulk Ge with a 10 % laser power.

Having demonstrated the significance of TDD reduction in enhancing the PL of Ge, we explored a Ge wafer with the lowest known TDD sourced from Umicore, claiming zero TDD characterized by EPD. Additionally, the P doping concentration can be increased to $5 \times 10^{17} \text{ cm}^{-3}$, potentially further amplifying the PL through a synergistic combination of low TDD and high P doping.

In Figure 4a, the photo of the Umicore bulk Ge is shown, with the corresponding 3D optical profilometer image of the polished side depicted in Figure 4b, revealing a Sq of $1 \pm 0.1 \text{ nm}$. The unpolished side of the Umicore bulk Ge is presented in Figure 4c, and its 3D optical profilometer image is displayed in Figure 4d, illustrating a Sq of $8.2 \pm 0.3 \text{ nm}$. Figure 4e compares the PL intensity between UW bulk Ge (TDD = 6000 cm^{-2}), epi-Ge, and Umicore bulk Ge. Impressively, the PL intensity from Umicore bulk Ge is much higher than that from UW bulk Ge, which is ten times higher than that from epi-Ge.

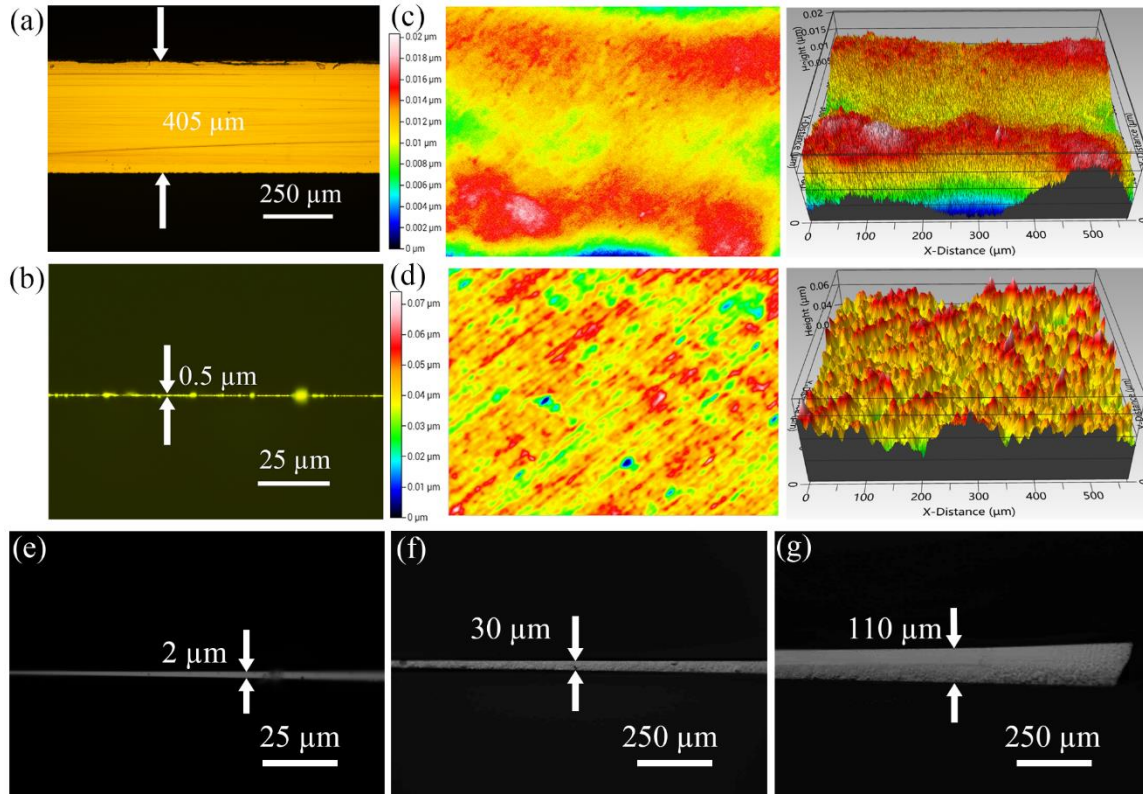


Figure 5. (a) The thickness of the Umicore Ge wafer before the wet etching, (b) the thickness of the Umicore Ge thin film after the wet etching, (c) the 3D optical profilometer image from the polished side after the wet etching, (d) the 3D optical profilometer image from the unpolished side after the wet etching, (e) the cross-section near the top, thin edge (f) the cross-section near the middle part, medium region, (g) the cross-section near the bottom, thick region

Using the wet etching method, the Umicore bulk Ge was thinned down to enhance the PL intensity further. The initial thickness before etching is shown in Figure 5a, and after etching, the thickness at the top is reduced to $0.5\ \mu\text{m}$ (Figure 5b). The 3D optical profilometer image from the polished side post-etching is presented in Figure 5c, displaying a Sq of $1.9 \pm 0.3\ \text{nm}$. The 3D optical profilometer image from the unpolished side is shown in Figure 5d, with a Sq of $7.4 \pm 2.1\ \text{nm}$. Figures 5e-5g show the thickness variation from the top to the bottom, demonstrating a sword shape. Figure 6a illustrates the PL from the Umicore bulk before and after wet etching. The PL intensity consistently increases with decreasing thickness, resembling the trend observed in university bulk Ge. Remarkably, after thinning the bulk Ge to $\sim 1\ \mu\text{m}$ (near the top), the intensity increases to 12 times that of epi-Ge on Si (Figure 6b). Notably, the thickness influence in Umicore bulk Ge is less pronounced than in the UW Wafer, which is attributed to the significantly lower TDD in the Umicore wafer. This underscores TDD as a more crucial factor than the thickness and n-doping for high-quality Ge in PL measurements.

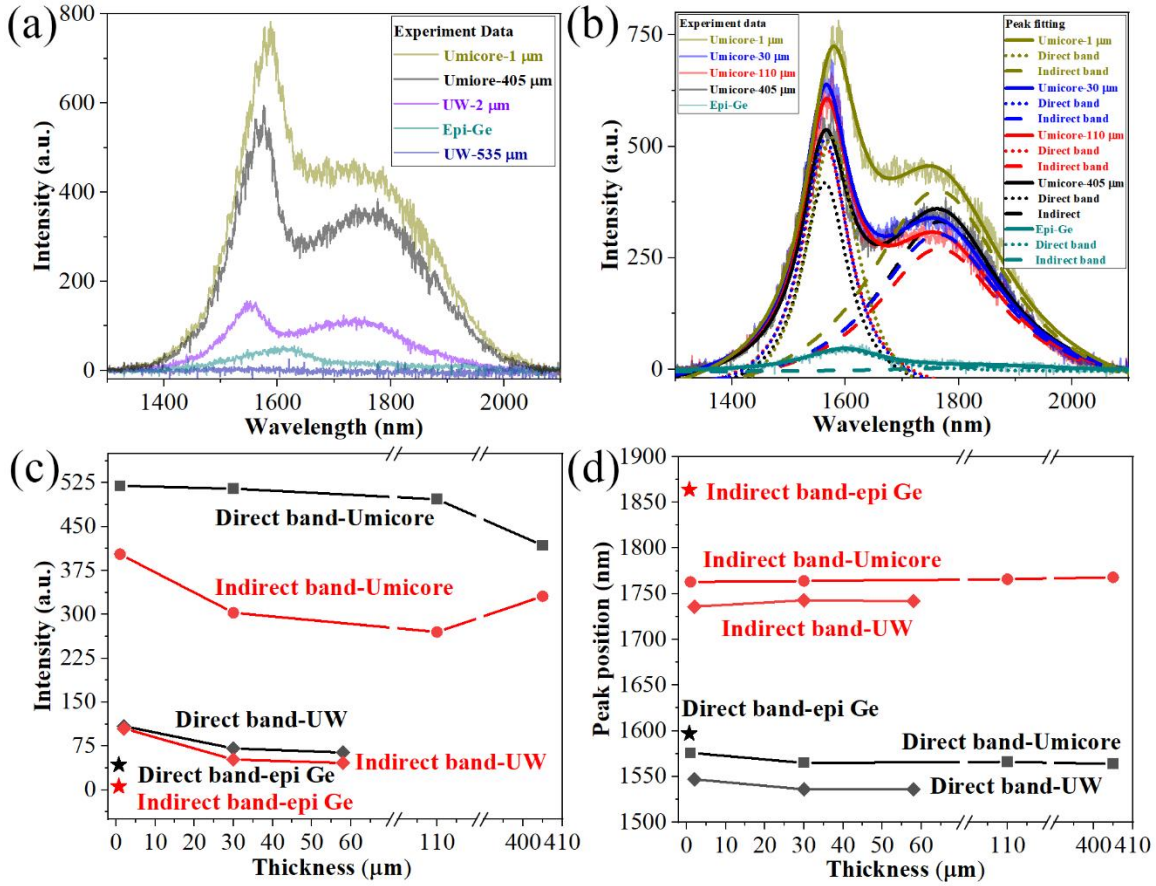


Figure 6. (a) The PL of the Umicore bulk Ge and Umicore Ge thin film with different thicknesses, (b) the fitted PL peaks of the Umicore bulk Ge and Umicore Ge thin film with different thicknesses, (c) the PL intensity vs Ge thickness, and (d) the PL peak position vs Ge thickness.

3.3.1 PL excitation laser power dependence of the Umicore Ge film PL spectra

It is noted that the direct band emission at the Umicore Ge-1 μm shifted to 1576 nm from the original ~ 1565 nm due to the heating effect. To avoid the heating effect of the measurement, the power dependence of Ge thin edge is shown in Figure 7a. The PL intensity keeps increasing when the power increases from 5 % to 10 % to 25 %. Considering the peak position, the laser power of 5 % could be a better choice to decrease the heating effect. Figure 7d presents a linear scan of the PL measurement near the edge of the Ge thin film. The intensity exhibits an increasing trend as the thickness is reduced for values higher than 0.9 μm . However, as the thickness further decreases to 0.7 μm , there is a subsequent decrease in PL intensity. Considering the penetration depth of 1064

nm in Ge is approximately 1 μm , it suggests that a thickness of around 1 μm might be optimal for PL measurements. This thickness strikes a balance between having sufficient thickness for a robust signal and a lower thickness to mitigate self-absorption effects.

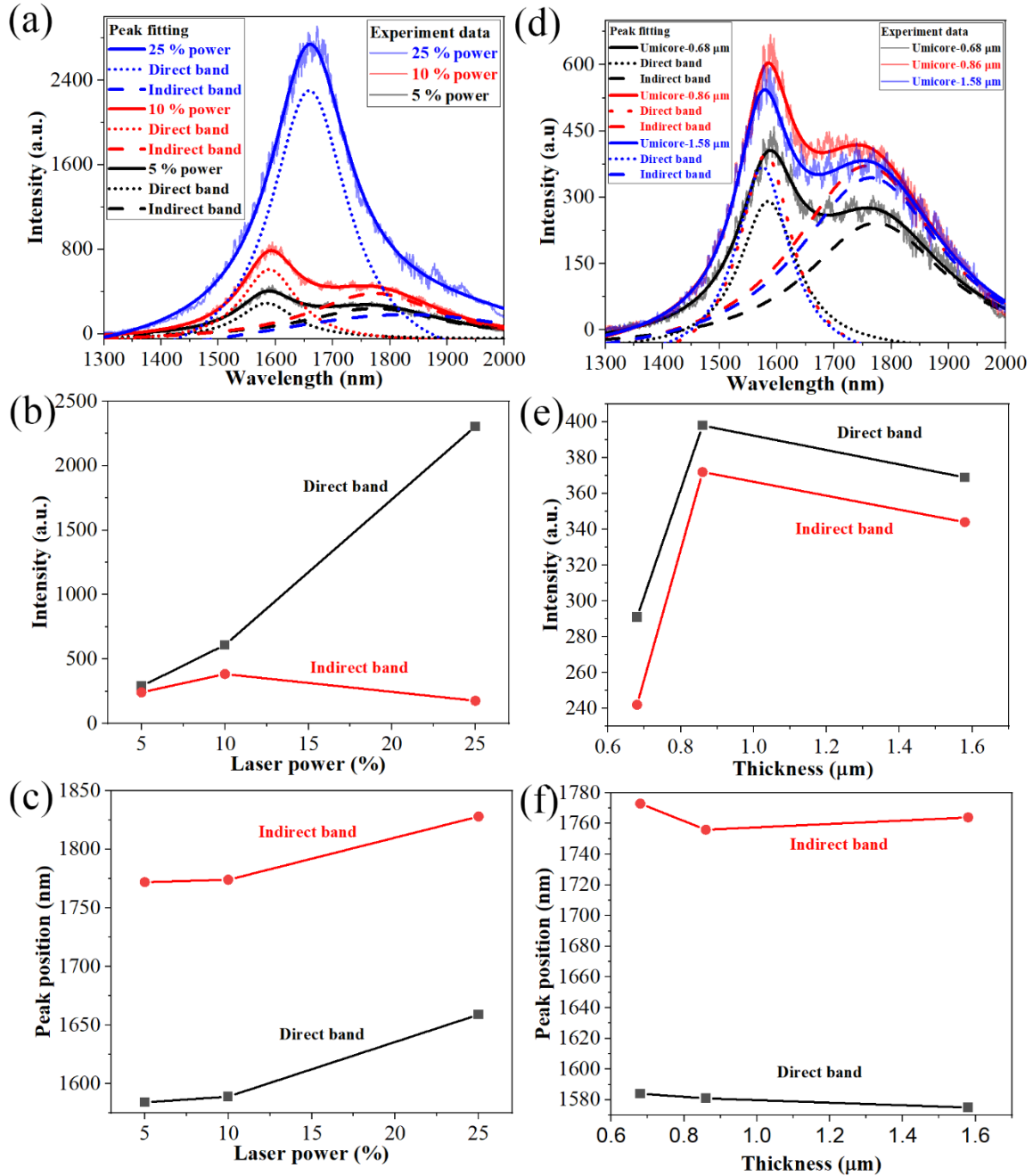


Figure 7. (a) The laser power dependence near the top of the Umicore thin film, (b) the PL intensity vs. laser power, (c) the PL peak position vs laser power, (d) the PL of the Umicore Ge thin film near the top, with 5 %

laser power, (e) the PL intensity vs the thickness near the top at 5 % laser power, and (f) the PL peak position vs the thickness near the top at 5 % laser power.

3.3.2 Surface roughness dependence of the Umicore Ge film PL

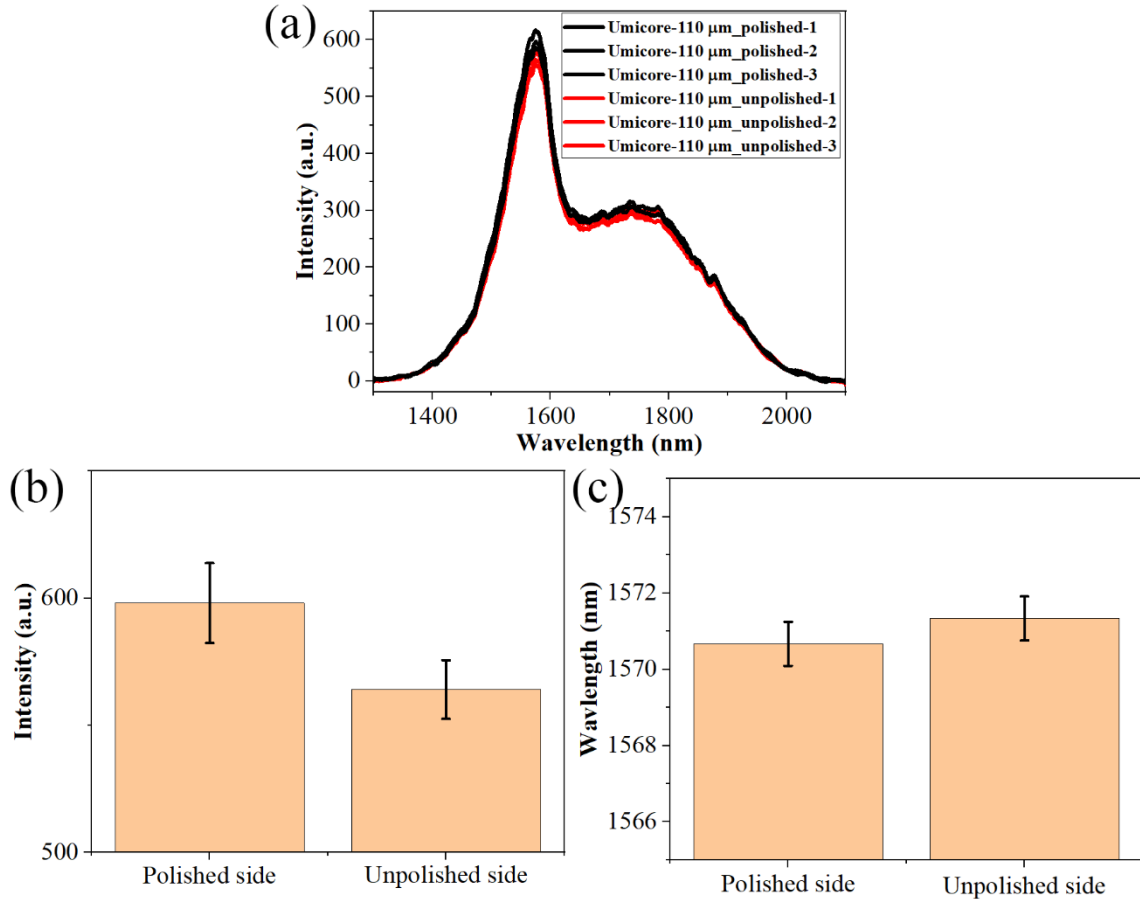


Figure 8. (a) The PL from both sides of the Umicore Ge-110 μm (S_q of the polished side = 1.9 ± 0.3 nm, S_q of the unpolished side = 7.4 ± 2.1 nm), (b) the peak intensity from both sides, (c) the peak position from both sides.

A key consideration in wet etching is understanding whether surface roughness plays a role in determining PL intensity. We compared the Umicore-110 μm on both sides, as depicted in Figure 8a to investigate this. Surprisingly, there is no noticeable difference in peak shape, indicating that surface roughness does not significantly influence it. Furthermore, there is no discernible difference in peak position, suggesting that surface roughness does not contribute to the peak position. The difference is subtle, while the PL intensity shows a minor increase ($\sim 5\%$) on the front side with

lower surface roughness. This observation suggests that surface roughness can play a role in PL intensity but is a minor contributing factor. Despite the significant difference in surface roughness, the impact on PL intensity remains relatively small.

4. Conclusions

In this study, we illustrated that the PL peak intensity of a UW bulk Ge sample (535 μm thick, TDD = 6000 cm^{-2} , n-doping = $1 \times 10^{16} \text{ cm}^{-3}$) can be significantly enhanced by 32 times by reducing the thickness to 2 μm by wet etching. Capitalizing on the superior Ge quality, even with a 1.25 μm more thickness, and 1/1000 of the n-doping, the PL peak intensity of the 2- μm -thick UW bulk Ge sample, surpasses that of the bench-marking epi-Ge sample (0.75 μm thick, TDD $\sim 10^8 \text{ cm}^{-3}$, biaxial tensile strain = 0.2 %, n-doping = $1 \times 10^{19} \text{ cm}^{-3}$) by a factor of 2.5, demonstrating the critical role of TDD reduction in PL intensity enhancement. Furthermore, our ultra-low-TDD Umicore Ge thin film (1 μm thick, TDD = 0, n-doping = $5 \times 10^{17} \text{ cm}^{-3}$) achieved 12 times the PL intensity of the bench-marking epi-Ge (0.75 μm thick, TDD $\sim 10^8 \text{ cm}^{-3}$, biaxial tensile strain = 0.2 %, n-doping = $1 \times 10^{19} \text{ cm}^{-3}$), which has 20 times of n-type doping. The change from 1.9 to 7.4 nm surface roughness doesn't change the PL shape and position and only decreased the PL intensity by 5%.

The ultra-low-TDD Ge approach also mitigates the side effects of high optical absorption, high recombination rates, and bandgap narrowing associated with the high n-type doping method and the larger footprint and bandgap narrowing associated with the stress concentration method. The use of ultra-low-TDD bulk Ge wafers as the starting materials was proved to overcome the technology barrier of high-TDDs in epi-Ge on Si, and provides a new solution to on-chip Ge lasers.

Author contributions

Liming Wang: conceptualization, methodology, investigation, writing original draft, writing-review & editing, visualization. Gideon Kassa: investigation. Jifeng Liu: research supervision,

resources, writing- review & editing. Guangrui (Maggie) Xia: conceptualization, research supervision, resources, writing – review & editing.

Conflicts of interest

There are no conflicts to declare.

Acknowledgement

We gratefully acknowledge CMC Microsystems for providing MNT Awards to cover fabrication costs. Our thanks extend to UBC nanofab for their invaluable training and assistance with cleanroom equipment. Additionally, we express our gratitude to Umicore Wafer for their support. Liming Wang acknowledges the financial support received from the UBC Four Year Doctoral Fellowship and the Natural Sciences and Engineering Research Council of Canada (NSERC).

References

1. Wu, J.; Lin, X.; Guo, Y.; Liu, J.; Fang, L.; Jiao, S.; Dai, Q., Analog optical computing for artificial intelligence. *Engineering* **2022**, *10*, 133-145.
2. Fan, X.; White, I. M.; Zhu, H.; Suter, J. D.; Oveys, H. In *Overview of novel integrated optical ring resonator bio/chemical sensors*, Laser Resonators and Beam Control IX, SPIE: **2007**; pp 166-185.
3. De Leon, N. P.; Itoh, K. M.; Kim, D.; Mehta, K. K.; Northup, T. E.; Paik, H.; Palmer, B.; Samarth, N.; Sangtawesin, S.; Steuerman, D. W., Materials challenges and opportunities for quantum computing hardware. *Science* **2021**, *372* (6539), eabb2823.
4. Blaicher, M.; Billah, M. R.; Kemal, J.; Hoose, T.; Marin-Palomo, P.; Hofmann, A.; Kutuvantavida, Y.; Kieninger, C.; Dietrich, P.-I.; Lauermann, M., Hybrid multi-chip assembly of optical communication engines by in situ 3D nano-lithography. *Light: Science & Applications* **2020**, *9* (1), 71.

5. Zhou, Z.; Ou, X.; Fang, Y.; Alkhazraji, E.; Xu, R.; Wan, Y.; Bowers, J. E., Prospects and applications of on-chip lasers. *Elight* **2023**, *3* (1), 1-25.
6. Tang, M.; Park, J.-S.; Wang, Z.; Chen, S.; Jurczak, P.; Seeds, A.; Liu, H., Integration of III-V lasers on Si for Si photonics. *Progress in Quantum Electronics* **2019**, *66*, 1-18.
7. Sun, X.; Liu, J.; Kimerling, L. C.; Michel, J., Toward a germanium laser for integrated silicon photonics. *IEEE Journal of Selected Topics in Quantum Electronics* **2009**, *16* (1), 124-131.
8. Bao, S.; Kim, D.; Onwukaeme, C.; Gupta, S.; Saraswat, K.; Lee, K. H.; Kim, Y.; Min, D.; Jung, Y.; Qiu, H., Low-threshold optically pumped lasing in highly strained germanium nanowires. *Nature communications* **2017**, *8* (1), 1845.
9. Saraswat, K.; Chui, C. O.; Krishnamohan, T.; Kim, D.; Nayfeh, A.; Pethe, A., High performance germanium MOSFETs. *Materials Science and Engineering: B* **2006**, *135* (3), 242-249.
10. Khanday, M. A.; Bashir, F.; Khanday, F. A., Single germanium MOSFET-based low energy and controllable leaky integrate-and-fire neuron for spiking neural networks. *IEEE Transactions on Electron Devices* **2022**, *69* (8), 4265-4270.
11. Michel, J.; Liu, J.; Kimerling, L. C., High-performance Ge-on-Si photodetectors. *Nature photonics* **2010**, *4* (8), 527-534.
12. Zhou, D.; Chen, G.; Fu, S.; Zuo, Y.; Yu, Y., Germanium photodetector with distributed absorption regions. *Optics Express* **2020**, *28* (14), 19797-19807.
13. Fujikata, J.; Noguchi, M.; Kawashita, K.; Katamawari, R.; Takahashi, S.; Nishimura, M.; Ono, H.; Shimura, D.; Takahashi, H.; Yaegashi, H., High-speed Ge/Si electro-absorption optical modulator in C-band operation wavelengths. *Optics express* **2020**, *28* (22), 33123-33134.
14. Benedikovic, D.; Virost, L.; Aubin, G.; Hartmann, J.-M.; Amar, F.; Le Roux, X.; Alonso-Ramos, C.; Cassan, É.; Marris-Morini, D.; Fédéli, J.-M., Silicon–germanium receivers for short-

wave-infrared optoelectronics and communications: High-speed silicon–germanium receivers (invited review). *Nanophotonics* **2020**, *10* (3), 1059-1079.

15. Sánchez-Pérez, J. R.; Boztug, C.; Chen, F.; Sudradjat, F. F.; Paskiewicz, D. M.; Jacobson, R.; Lagally, M. G.; Paiella, R., Direct-bandgap light-emitting germanium in tensilely strained nanomembranes. *Proceedings of the National Academy of Sciences* **2011**, *108* (47), 18893-18898.

16. Liu, J.; Sun, X.; Pan, D.; Wang, X.; Kimerling, L. C.; Koch, T. L.; Michel, J., Tensile-strained, n-type Ge as a gain medium for monolithic laser integration on Si. *Optics express* **2007**, *15* (18), 11272-11277.

17. Camacho-Aguilera, R. E.; Cai, Y.; Patel, N.; Bessette, J. T.; Romagnoli, M.; Kimerling, L. C.; Michel, J., An electrically pumped germanium laser. *Optics express* **2012**, *20* (10), 11316-11320.

18. Ke, J.; Chrostowski, L.; Xia, G., Stress engineering with silicon nitride stressors for Ge-on-Si lasers. *IEEE Photonics Journal* **2017**, *9* (2), 1-15.

19. Li, X.; Li, Z.; Li, S.; Chrostowski, L.; Xia, G. M., Design considerations of biaxially tensile-strained germanium-on-silicon lasers. *Semiconductor Science and Technology* **2016**, *31* (6), 065015.

20. Son, B.; Lin, Y.; Lee, K. H.; Chen, Q.; Tan, C. S., Dark current analysis of germanium-on-insulator vertical pin photodetectors with varying threading dislocation density. *Journal of Applied Physics* **2020**, *127* (20).

21. Geiger, R.; Frigerio, J.; Süess, M.; Chrastina, D.; Isella, G.; Spolenak, R.; Faist, J.; Sigg, H., Excess carrier lifetimes in Ge layers on Si. *Applied Physics Letters* **2014**, *104* (6).

22. Sun, X. Ge-on-Si light-emitting materials and devices for silicon photonics. Massachusetts Institute of Technology, **2009**.

23. Haynes, J.; Nilsson, N. In *The direct radiative transitions in germanium and their use in the analysis of lifetime*, Proceedings of VIIth International Conference on Physics of Semiconductors, **1964**; p 21.

24. Letertre, F.; Deguet, C.; Richtarch, C.; Faure, B.; Hartmann, J.; Chieu, F.; Beaumont, A.; Dechamp, J.; Morales, C.; Allibert, F., Germanium-on-insulator (GeOI) structure realized by the Smart Cut™ technology. *MRS Online Proceedings Library (OPL)* **2004**, 809.
25. Peaker, A. R.; Markevich, V.; Slotte, J.; Rummukainen, M.; Capan, I.; Pivac, B.; Gwilliam, R.; Jeynes, C.; Dobaczewski, L., Understanding ion implantation defects in germanium. *ECS Transactions* **2006**, 3 (2), 67.
26. Camacho-Aguilera, R. E. Ge-on-Si laser for silicon photonics. Massachusetts Institute of Technology, **2013**.
27. Wang, L.; Xia, G., Ultrahigh-Quality Ge-on-Glass with a 3.7% Uniaxial Tensile Strain. *ACS Omega* **2024**.
28. El Kurdi, M.; Bertin, H.; Martincic, E.; De Kersauson, M.; Fishman, G.; Sauvage, S.; Bosseboeuf, A.; Boucaud, P., Control of direct band gap emission of bulk germanium by mechanical tensile strain. *Applied Physics Letters* **2010**, 96 (4).
29. Wang, L.; Zhu, Y.; Wen, R.-T.; Xia, G., Sub-10 μm-Thick Ge Thin Film Fabrication from Bulk-Ge Substrates via a Wet Etching Method. *ACS Omega* **2023**, 8 (51), 49201-49210.
30. Zhou, G.; Covian, A. V. C.; Lee, K. H.; Han, H.; Tan, C. S.; Liu, J.; Xia, G. M., Improved thin film quality and photoluminescence of N-doped epitaxial germanium-on-silicon using MOCVD. *Optical Materials Express* **2020**, 10 (1), 1-13.
31. El Kurdi, M.; Kociniowski, T.; Ngo, T.-P.; Boulmer, J.; Débarre, D.; Boucaud, P.; Damlencourt, J.; Kermarrec, O.; Bensahel, D., Enhanced photoluminescence of heavily n-doped germanium. *Applied Physics Letters* **2009**, 94 (19).